# CFD Simulation of Liquid–Phase Mixing in Solid–Liquid Stirred Reactor

**Article** *in* Chemical Engineering Science · August 2008

DOI: 10.1016/j.ces.2008.04.018

CITATIONS
228

READS
1,138

**4 authors:**

Gopal Kasat
Independent Researcher
**16** PUBLICATIONS **664** CITATIONS
SEE PROFILE

Avinash r Khopkar
Reliance Industries Limited
**31** PUBLICATIONS **1,170** CITATIONS
SEE PROFILE

Vivek V. Ranade
Queen's University Belfast
**186** PUBLICATIONS **8,229** CITATIONS
SEE PROFILE

Aniruddha Bhalchandra Pandit
Institute of Chemical Technology
**573** PUBLICATIONS **32,471** CITATIONS
SEE PROFILE

Chemical Engineering Science 63 (2008) 3877 – 3885

Contents lists available at ScienceDirect

Chemical Engineering Science

journal homepage: www.elsevier.com/locate/ces

# CFD simulation of liquid-phase mixing in solid–liquid stirred reactor

G.R. Kasat[a], A.R. Khopkar[b], V.V. Ranade[b,*], A.B. Pandit[a]

[a]Institute of Chemical Technology, University of Mumbai, Mumbai 400 019, India
[b]Industrial Flow Modeling Group, National Chemical Laboratory, Pune 411 008, India

ARTICLE INFO

*Article history:*
Received 4 July 2006
Received in revised form 3 April 2008
Accepted 9 April 2008
Available online 11 June 2008

*Keywords:*
Stirred reactor
CFD
Solid suspension
Mixing

ABSTRACT

A comprehensive CFD model was developed to gain an insight into solid suspension and its implications on the liquid-phase mixing process in a solid–liquid stirred reactor. The turbulent solid–liquid flow in a stirred reactor was simulated using a two-fluid model with the standard $k$–$\varepsilon$ turbulence model with mixture properties. The multiple reference frames (MRFs) approach was used to simulate impeller rotation in a fully baffled reactor. The computational model with necessary sub-models was mapped on to a commercial solver FLUENT 6.2 (of Fluent Inc., USA). The predicted solid concentration distribution was compared with the experimental data of Yamazaki et al. [1986. Concentration profiles of solids suspended in a stirred tank. Powder Technology 48, 205–216]. The computational model was then further extended to simulate and understand the implications of the suspension quality on liquid-phase mixing process. The computational model and the predicted results discussed here will be useful for understanding the liquid-phase mixing process in stirred slurry reactors in various stages of solid suspension.



## 1. Introduction

Solid–liquid stirred reactors are widely used in the chemical process industry for variety of operations such as catalytic reactions, crystallization, leaching, polymerization, etc. The performance of the solid–liquid stirred reactor is controlled by the suspension quality prevailing in the reactor and the liquid-phase mixing process. In a stirred tank reactor, mixing is a very complex process and is achieved through convection and turbulent exchanges. This complex process can be distinguished and described into two simpler stages of mixing i.e., macro-mixing (mixing at the scale of whole reactor) and micro-mixing (mixing at molecular scale). Chemical reaction is a molecular level process and only micro-mixing can affects its course directly. However, the environment for the micro-mixing is defined by macro-mixing (Baldyga and Pohorecki, 1995) and hence the information related to macro-mixing is also very important to control the performance of a chemical reaction. It is therefore essential to have the knowledge of macro-mixing time before studying the micro-mixing.

In case of stirred slurry reactor, uncharacteristic trend was observed in dimensionless macro-mixing time variation with impeller rotational speed. In many cases, solid–liquid stirred reactors are operated with high solid loading (having solid volume fraction $> 5.0\%$). In such situations, the liquid-phase mixing process has been found to show a complex interaction with the suspension quality (Kraume, 1992; Harrop et al., 1997; Bujalski et al., 1999; Michelletti et al., 2003). It was observed that the characteristic time scale of the mixing process commonly known as *mixing time* shows a typical trend depending upon the suspension quality and/or impeller rotational speed. For incomplete suspension regime, the mixing time was first found to increase with impeller rotational speed till the maximum value (more than 7 times of the minimum value) is reached and then drops gradually with further increase in the impeller rotational speed till the just off-bottom suspension condition is reached. The mixing time was then found to remain constant till the system approaches complete suspension condition and then the mixing time slowly reduces with further increase in impeller rotational speed.

The reported literature show significant uncertainties over the exact identification of the operating conditions at which the maximum mixing time has been observed. Earlier studies (Kraume, 1992; Harrop et al., 1997; Bujalski et al., 1999) have reported that maximum in the mixing time was observed at an impeller speed just below the critical impeller speed for just suspension (Njs). Whereas, the recent study of Michelletti et al. (2003) have observed the maximum in the mixing time at an impeller speed equal to $\frac{1}{3}$rd of Njs. However, all the studies (Kraume, 1992; Harrop et al., 1997; Bujalski et al., 1999; Michelletti et al., 2003) unanimously suggested the late occurrence of mixing in the top clear liquid layer as a major reason for the observed increase in the overall fluid mixing time.

The difficulties experienced during the measurement of mixing time in the dense suspension might be a possible reason for this

* Corresponding author. Tel./fax: +91 20 25902 170.
*E-mail address:* vv.ranade@ncl.res.in (V.V. Ranade).

0009-2509/$ - see front matter © 2008 Elsevier Ltd. All rights reserved.
doi:10.1016/j.ces.2008.04.018

observed discrepancy. In all the reported studies, the authors were able to measure the mixing time in the clear liquid layer and not in the slurry. This may be one of the reasons of correlating the observed increase in the mixing time only with the delayed mixing in the clear liquid layer above the level of the dense suspension. Considering the discrepancies in the published experimental studies, it becomes essential to use the available computational models to first understand the mixing on macro-scale before inspecting it on molecular scale. The present study was therefore carried out to increase the understanding on the mixing process, identify the operating conditions at which maximum mixing time is possible and the reason behind the observed delayed mixing in a solid–liquid stirred reactor.

In the present work, a computational fluid dynamics (CFD) based model was used to understand the complex interactions between the suspension quality and the fluid mixing process. Khopkar et al. (2006) have presented a computational approach to simulate solid suspension in a stirred reactor for a wide range of operating conditions. The similar approach was used to simulate the solid–liquid flows generated by Rushton turbine. The model predictions were compared with the experimental data of axial solid concentration profile reported by Yamazaki et al. (1986). The validated model was then further extended to simulate the liquid-phase macro-mixing process in the solid–liquid stirred reactor. The model predictions were used to understand the interaction of the suspension quality and the liquid-phase mixing process. The details of the computational model as well as the results obtained are discussed in the following sections.

## 2. Computational model

### 2.1. Model equations

Most of the applications involving solid–liquid flows in stirred reactor are in turbulent regime. Therefore, the Reynolds averaged mass and momentum balance equations for any phase $q$ in turbulent flow regime were written as (without considering mass transfer)

$$\frac{\partial(\alpha_q\rho_q)}{\partial t} + \nabla(\alpha_q\rho_q\overrightarrow{U}_{q,i}) = 0 \tag{1}$$

$$\frac{\partial(\alpha_q\rho_q\overrightarrow{U}_{q,i})}{\partial t} + \nabla(\alpha_q\rho_q\overrightarrow{U}_{q,i}\times\overrightarrow{U}_{q,i}) = -\alpha_q\nabla p - \nabla(\alpha_q\bar{\bar{\tau}}^{(\mathrm{lam})}_{q,ij}) - \nabla(\alpha_q\bar{\bar{\tau}}^{(t)}_{q,ij}) + \alpha_q\rho_q g_i + \overrightarrow{F}_{td} + \overrightarrow{F}_{12,i} \tag{2}$$

Here $q = 1$ and 2 denote the continuous phase (liquid) and the suspended phase (solid), respectively, and $i$ is the direction. $\overrightarrow{U}_q$ and $\alpha_q$ are the time-averaged values of the velocity and volume fraction of phase $q$, respectively. It should be noted that time-averaged pressure, $p$, is shared by both the phases and therefore appears in the governing equations of all the phases. $\rho_q$ is the density of the phase and $\alpha_q\rho_q g_i$ is the external body force on the phase $q$. $\overrightarrow{F}_{td}$ denotes the turbulent dispersion force accounting for the fluctuations in the phase volume fraction $\overrightarrow{F}_{12,i}$ is the time-averaged inter-phase force in $i$ direction. Modeling of these two forces is discussed in detail later in this section. $\bar{\bar{\tau}}^{(\mathrm{lam})}_{q,ij}$ is the stress tensor in the phase $q$ due to the viscosity. $\bar{\bar{\tau}}^{(t)}_{q,ij}$ is the additional term which appears in the momentum equation due to the Reynolds averaging and is known as Reynolds stress. It represents the effect of turbulent fluctuations on the convective transport over the averaging time period. The Reynolds stresses needs to be modeled in order to close the set of equations. In the present study, we used Boussinesq's eddy viscosity hypothesis to relate the Reynolds stresses for phase $q$ with gradients of time-averaged velocity for phase $q$ as

$$\bar{\bar{\tau}}^{(t)}_{q,ij} = \mu_{tm}((\nabla\overrightarrow{U}_{q,i} + (\nabla\overrightarrow{U}_{q,i})^{\mathrm{T}}) - \frac{2}{3}I(\nabla\overrightarrow{U}_{q,i})) \tag{3}$$

where, $\mu_{tm}$ is the turbulent viscosity of mixture and $I$ is the unit stress tensor. In the present study, the $k$–$\varepsilon$ mixture turbulence was used for modeling the turbulence and hence the turbulent viscosity is taken for the mixture. The basis for choosing the $k$–$\varepsilon$ mixture turbulence model and its formulation is discussed below.

Different turbulence models are available in the literature to estimate the turbulent viscosity. Most of the researchers have used the standard $k$–$\varepsilon$ turbulence model for simulating single as well as multi-phase flows in stirred vessels. The standard $k$–$\varepsilon$ turbulence model, however, does not predict the turbulent quantities accurately for rotating flows. Derksen (2003) has used large eddy simulations (LES) to simulate the solid suspension in stirred tanks. Such simulations, however, still require a significant amount of CPU time and therefore are not yet fine-tuned for quick process design validation. Also, such simulations have not yet been validated for the higher solid concentrations of the slurries. The numerical study of Jenne and Reuss (1999) have indicated that different time scales and anisotropy consideration are of minor importance and do not lead to significant improvement over standard $k$–$\varepsilon$ turbulence model.

The use of RANS based standard $k$–$\varepsilon$ turbulence model may also not be adequate to capture the tracer concentration history (discussed latter) which, in the present study, is used to calculate the liquid-phase mixing time and LES approach is needed to capture the realistic tracer concentration history. It should, however, be noted that the objective of the present work was not to capture tracer concentration history accurately but was to predict the overall liquid-phase mixing time in the reactor so as to understand the influence of suspension quality on the liquid-phase mixing process. The overall mixing time predicted using the tracer concentration history simulated with the RANS based standard $k$–$\varepsilon$ turbulence model has been shown to be in reasonable agreement with single-phase experimental data (see Ranade, 2002 and references cited therein). Following the recommendations of Jenne and Reuss (1999) and Ranade (2002), the RANS based $k$–$\varepsilon$ turbulence model is used for simulating solid–liquid flows and liquid-phase mixing time in the stirred reactor.

For simulating turbulence in multi-phase systems, three different extensions of standard $k$–$\varepsilon$ turbulence model (mixture, per phase or dispersed) are available. In the mixture formulation, only a couple of $k$ and $\varepsilon$ equations are solved, where the physical properties of the mixture are adopted and the two phases are assumed to share the same $k$ and $\varepsilon$ values. In the per phase approach, the turbulence model equations are solved for all the phases present. Alternatively, in a third approach, turbulence is first simulated for continuous phase and then Tchen's theory is used to estimate the turbulent quantities of the dispersed phase. Montante and Magelli (2005) have studied the influence of these three formulations on predicted results. They have observed that using more computationally demanding approaches like per phase formulation does not lead to any significant improvement over the mixture formulation. Following their recommendation, in the present study we have used the $k$–$\varepsilon$ mixture turbulence model to model the turbulence in the solid–liquid stirred reactor.

The governing equations for turbulent kinetic energy, $k$ and turbulent energy dissipation rate, $\varepsilon$, are listed below:

$$\frac{\partial}{\partial t}(\rho_m\phi) + \nabla(\rho_m\overrightarrow{U}_{m,i}\phi) = -\nabla\left(\frac{\mu_{tm}}{\sigma_{\phi m}}\nabla\phi\right) + S_\phi \tag{4}$$

where the mixture density and velocity were calculated as

$$\rho_m = \sum_{q=1}^{n} \alpha_q \rho_q \tag{5}$$

$$\vec{U}_m = \frac{\sum_{q=1}^{n} \alpha_q \rho_q \vec{U}_q}{\sum_{q=1}^{n} \alpha_q \rho_q} \tag{6}$$

The turbulent viscosity for mixture, $\mu_{tm}$ is computed from

$$\mu_{tm} = \frac{\rho_m C_\mu k^2}{\varepsilon} \tag{7}$$

The property $\phi$ can be turbulent kinetic energy or turbulent energy dissipation rate for a mixture. The symbol $\sigma_\phi$ denotes turbulent Prandtl number for variable $\phi$. $S_\phi$ is the corresponding source term for $\phi$ of mixture. Source terms for turbulent kinetic energy, $k$ and turbulent dissipation rate $\varepsilon$ can be written as

$$S_k = G - \rho_m \varepsilon, \quad S_\varepsilon = \frac{\varepsilon}{k}[C_1 G - C_2 \rho_m \varepsilon] \tag{8}$$

where $G$ is the generation of turbulence in the mixture and was calculated as

$$G = \frac{1}{2}\mu_{tm}(\nabla \vec{U}_{m,i} + (\nabla \vec{U}_{m,i})^{\mathrm{T}})^2 \tag{9}$$

In all the simulations, standard values of the $k$–$\varepsilon$ model parameters were used in the present simulations ($C_1 = 1.44$, $C_2 = 1.92$, $C_\varpi = 0.09$, $\sigma_k = 1.0$ and $\sigma_\varepsilon = 1.3$).

It should be noted that the contribution of turbulent dispersion force is significant only when the size of the turbulent eddies is larger than the particle size. In the case of solid–liquid stirred reactor, even for laboratory scale, the ratio of the largest energy containing eddy (in mm) and the particle size was found to be around 10. Therefore, the contribution of the turbulent dispersion is likely to be significant. The previously reported numerical studies have also highlighted the importance of modeling of turbulent dispersion force while simulating solid suspension in stirred reactor (Ljungqvist and Rasmuson, 2001; Angst et al., 2003; Barrue et al., 2001). Considering these results, the turbulent dispersion of the dispersed phase has been considered in the present study was modeled as a force in the momentum equation:

$$\vec{F}_{td} = KV_{\mathrm{dr}} \tag{10}$$

$$V_{\mathrm{dr}} = -\left(\frac{D_p}{\sigma_{pq}\alpha_p}\nabla\alpha_p - \frac{D_q}{\sigma_{pq}\alpha_q}\nabla\alpha_p\right) \tag{11}$$

Here, $V_{\mathrm{dr}}$ is the drift velocity; $D_p$ and $D_q$ are the diffusivities of the continuous and dispersed phase, respectively, and $\sigma_{pq}$ is the dispersion Prandtl number. In the present study $D_p$ and $D_q$ are calculated from the turbulent quantities following the work of Simonin and Viollet (1998) and the value of $\sigma_{pq}$ was taken as 0.75 (Fluent 6.2 users guide).

Inter-phase coupling terms make two-phase flows fundamentally different from single-phase flows. The formulation of time-averaged $\vec{F}_{12,i}$, therefore, must proceed carefully. The inter-phase momentum exchange term consists of four different inter-phase forces: lift force, Basset force, virtual mass force and drag force (Ranade, 1992). Basset force arises due to the development of a boundary layer around particles and is relevant only for unsteady flows. Basset force involves a history integral, which is time-consuming to evaluate and in most cases, its magnitude is much smaller than the inter-phase drag force. The influence of other inter-phase forces, such as lift force and virtual mass force on the simulated solid hold-up profile was studied by Ljungqvist and Rasmuson (2001). They have found very little influence of the virtual mass and lift force on the simulated solid hold-up profiles. Considering this, in the present work, Basset, lift and virtual mass forces were not considered and only the drag force term was included in the inter-phase momentum exchange term. Two-way coupling between the phases was considered and the inter-phase momentum exchange term was modeled as

$$\vec{F}_{12,i} = -\vec{F}_{12,i} = \vec{F}_{D,i} = -\frac{3\alpha_1\alpha_2\rho_1 C_D(\sum(\vec{U}_{2,i} - \vec{U}_{1,i})^2)^{0.5}(\vec{U}_{2,i} - \vec{U}_{1,i})}{4d_p} \tag{12}$$

In a solid–liquid stirred vessel, the inter-phase drag coefficient ($C_D$) is a complex function of the drag coefficient in a stagnant liquid ($C_{D0}$), the dispersed phase hold-up and prevailing bulk turbulence. Recently, Khopkar et al. (2006) studied the effect of turbulence on the drag coefficient using a two-dimensional sub-model. Based on the predicted results of the sub-model and the comparison of the predicted solid hold-up distribution in stirred reactor with the experimental data, they have recommended a turbulence correction factor suggested by Brucato et al. (1998) with the lower value of the correlation constant. Based on their study, we have used the following correlation for estimating the inter-phase drag coefficient, $C_D$:

$$\frac{C_D - C_{D0}}{C_{D0}} = 8.76 \times 10^{-5}\left(\frac{d_p}{\lambda}\right)^3 \tag{13}$$

where

$$C_{D0} = \frac{24}{Re_p} \times (1 + 0.15\,Re_p^{0.687}) \tag{14}$$

$\lambda$ is the Kolmogorov length scale, $d_p$ is the particle diameter. Eq. (12) thus accounts for the increased drag coefficient due to prevailing turbulence in the stirred reactor.

The interaction of the rotating impeller blades and of the stationary baffles generates an inherently unsteady flow. Recently, Ranade (2002) has reviewed various approaches for simulating the flow in a baffled stirred reactor. Following his recommendations, in the present study, multiple reference frames (MRFs) approach was used to simulate the impeller rotation in a fully baffled reactor. In this approach, the whole reactor is divided into two regions: an inner region attached to the rotating impeller and shaft and an outer region attached to the stationary baffles and the reactor. The model equations for the inner region are solved using a rotating framework (for this centrifugal and Coriolis forces were included in Eq. (2)), whereas the equations for the outer region are solved using a stationary framework. The time derivatives terms in Eqs. (1) and (2) are not solved while doing the steady state simulations using the MRF approach. The solution is matched at the interface between the rotating and stationary region via velocity transformation from one frame to the other.

### 2.2. Solution domain and boundary condition

In the present work, experimental setup used by Yamazaki et al. (1986) was considered for comparison and validation. The system investigated consists of a cylindrical, flat-bottomed reactor (of diameter, $T = 0.3$ m, liquid height, $H = T$). Four baffles of width $0.1T$ were mounted perpendicular to the reactor wall. The shaft of the impeller was concentric with the axis of the reactor and extended till the bottom of the reactor. The standard Rushton turbine (of diameter, $D = 0.1$ m) was used. The impeller off-bottom clearance was ($C = T/3$) measured from the level of the impeller disc. Following the experimental details of the Yamazaki et al. (1986), the dispersion of glass particles of mean diameter $d_p = 264\,\mu$m and density $\rho_s = 2470\,\mathrm{kg/m^3}$ suspended in water ($\rho_l = 1000\,\mathrm{kg/m^3}$; $\mu = 0.001\,\mathrm{kg/m\,s}$) at room

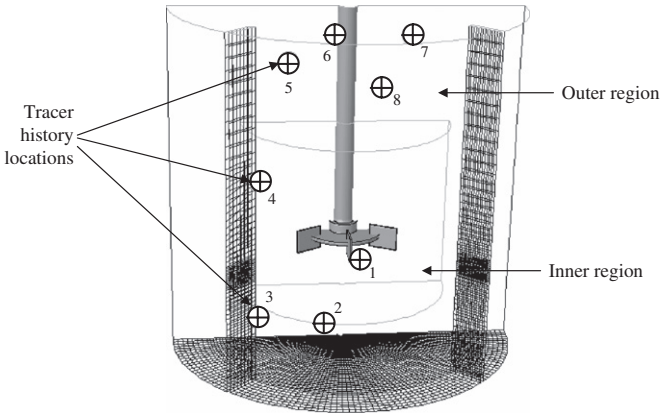


Grid Details :
r×θ× z : 57 × 93 × 57
Impeller blade: 14 × 1 × 14
Inner region : 8 ≤ k ≤ 47
j ≤ 39

| | x | y | z |
|---|---|---|---|
| Point-1 | -0.006 | 0.07 | 0.1 |
| Point-2 | 0.02 | 0.04 | 0.03 |
| Point-3 | 0.08 | 0.08 | 0.055 |
| Point-4 | 0.08 | 0.1 | 0.18 |
| Point-5 | 0.05 | 0.01 | 0.255 |
| Point-6 | 0.012 | 0.022 | 0.28 |
| Point-7 | -0.05 | 0.025 | 0.28 |
| Point-8 | -0.015 | 0.1 | 0.255 |

**Fig. 1.** Computational grid and solution domain of stirred reactor.

temperature was investigated. The mean solids concentration of 10% by volume was used in all the simulations. It should benoted that Yamazaki et al. (1986) have reported an average particle size equal to 264 μm in their experimental studies and the same value was used in the simulations discussed in this work.

Considering the periodicity of the flow, only half of the reactor was considered as a solution domain (see Fig. 1). The baffles were considered at angles of 45° and 135°. Impeller was positioned in such a way that three blades were located at angles of 30°, 90° and 150°. For modeling the impeller rotation MRF approach was used and the boundary of the inner region was positioned at $r = 0.09$ m and $0.05\,\text{m} \leqslant z \leqslant 0.20\,\text{m}$ (where $z$ is the axial distance from the bottom of the vessel). The initial condition for each simulation was that of still liquid and homogeneous distribution of solid particles inside the computational domain. The numerical solution of the equation system was obtained by using a commercial CFD solver Fluent 6.2 (Fluent Inc., USA). In the present work, QUICK discretization scheme with SUPERBEE limiter function (to avoid non-physical oscillations) was used. Standard wall functions were used to specify wall boundary conditions. In all the simulations, the volume fraction of solid-phase was not allowed to exceed maximum packing limit (0.63) by using a user defined function.

## 3. Result and discussion

### 3.1. Solid–liquid flow in stirred reactor

#### 3.1.1. Influence of grid size

The predictions of turbulent quantities are usually quite sensitive to the number of grid nodes used in the solution domain and thus it is very important to use an adequate number of computational cells while numerically solving the governing equations over the solution domain. In the present work, two grid sizes, 298 and 600 K, were considered to study the effect of grid size on predicted solid hold-up distribution. The predicted contour plots and profiles of solids concentration are shown in Fig. 2 of the revised manuscript. It can be seen that influence of grid size within the considered range was very small. The predicted values of volume averaged dissipation rate for these two grids were also within 2%. Based on these results, all the subsequent simulations were carried out with 298k computational cells for the half of the vessel.

#### 3.1.2. Solids hold-up distribution

The simulation of solid suspension in the stirred reactor was first carried out for particle size equal to 264 μm ($d_p/\lambda \approx 20$), total solid hold-up equal to 10% in the reactor and impeller rotational speed equal to 20 rps. It should be noted that for the present system, the onset of surface aeration was found to be at an impeller rotational speed equal to 11 rps (Van Dierendonck et al., 1968). However, in most of the experimental measurements, the vessel was covered with a top lid to avoid the surface aeration. In the present study, therefore, we have not considered the effect of surface aeration. However, the top lid was not considered in the simulation and the top surface of the liquid was modeled as free liquid surface with symmetry boundary conditions. The presence of very small magnitudes of the liquid velocities near the top surface leads to negligible differences in the results predicted with no-slip or free-slip boundary conditions at the top.

The predicted solid hold-up distribution (at mid-baffle plane) and the comparison of predicted angle-averaged values of the axial solid concentration profiles with the experimental data are shown in Fig. 3. It can be seen from Fig. 3 that the predicted solid hold-up distribution shows the accumulation of the solid particles around the central axis at the bottom of the vessel. However, in both the circulation loops almost uniform distribution of the solid particles was observed. The predicted solid hold-up distribution also show almost complete absence of solid particles near the top surface, indicating the presence of clear liquid layer above the level of the suspension. The comparison of the axial profile of azimuthally averaged solid hold-up values with the experimental data of Yamazaki et al. (1986) at radial location of $r/T = 0.35$ is also shown in Fig. 3. It can be seen from Fig. 3 that the computational model has reasonably captured the solids distribution in the stirred reactor.

The predicted values of the power number (calculated based on the skin and form drag experienced by the impeller) are shown in Table 1. It can be seen from Table 1 that the contribution of the skin drag experienced by the impeller in the over all power dissipated is very small (5–8%). The predicted power numbers appear to be under-predicted compared to the value of standard power number of the Rushton turbine (∼ 5).

#### 3.1.3. Suspension quality

In a solid–liquid stirred reactor, the prevailing suspension quality controls the liquid-phase mixing process. Therefore, it becomes essential first to adequately predict the quality of the suspension for different impeller rotational speeds. In a solid–liquid stirred reactor, the suspension quality can be identified viz. just off-bottom suspension, complete suspension and homogeneous suspension with respect to the impeller rotational speed. In the present study, the suspension of solid particles was simulated in stirred reactor for 11 impeller rotational speeds (starting from 2 to 40 rps) to study the effect of impeller rotational speed on the quality of suspension. Different criteria are available to characterize the suspension quality in the reactor. In the present study, the criteria based on the variation of the standard deviation of the solids concentration (Eq. (15)) with the impeller rotational speed was used to predict the quality of suspension prevailing in the reactor. Yamazaki et al. (1986) have not reported the values of $\sigma$ for their experiments. Due to the lack of experimental data, only qualitative prediction of the suspension quality is presented in this study. However, the definition of suspension quality used in the present study was based on the experimental

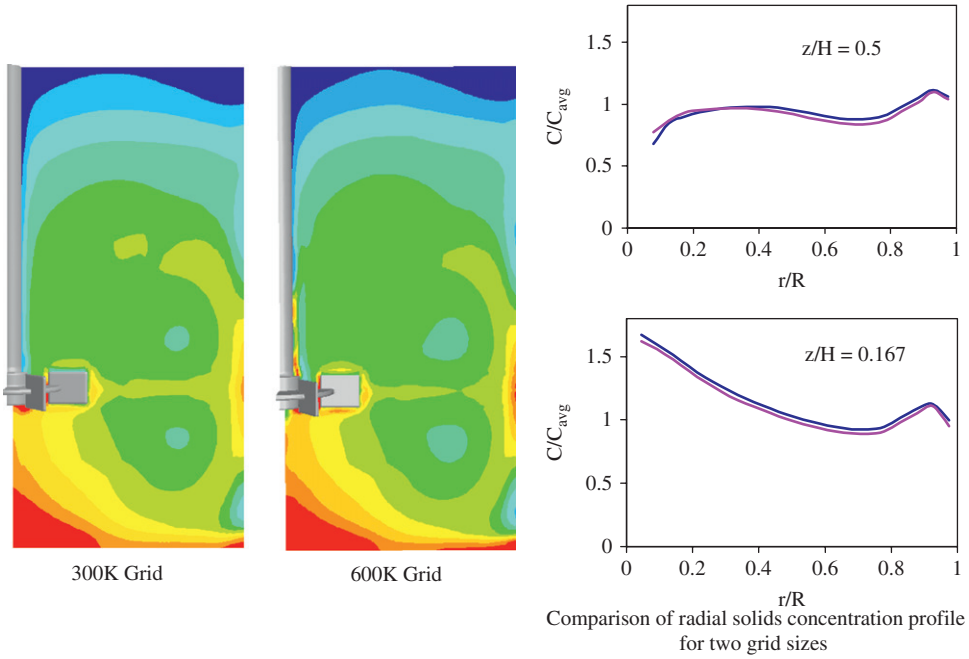


**Fig. 2.** Influence of grid size of predicted results, for $d_p = 264\,\mu m$, $N = 20.0$ rps.

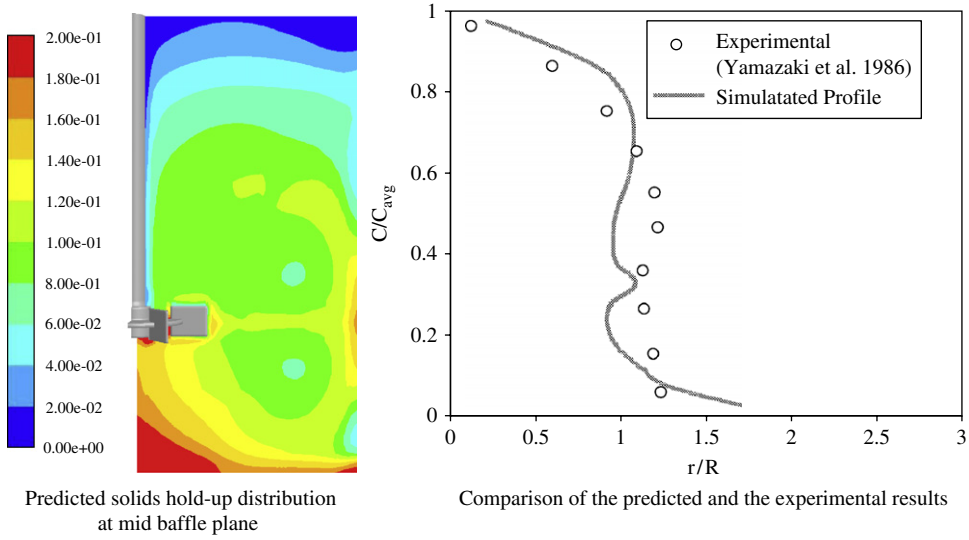


**Fig. 3.** Simulated solid hold-up distribution, for $d_p = 264\,\mu m$, $N = 20.0$ rps.

measurements of Bohnet and Niesmak (1980).

$$\sigma = \sqrt{\frac{1}{n}\sum_{i=1}^{n}\left(\frac{\alpha_{2i}}{\alpha_{2,\mathrm{avg}}} - 1\right)^2} \tag{15}$$

The variation in the predicted values of the standard deviation values with respect to impeller rotational speed are shown in Fig. 4. It can be seen from Fig. 4 that the standard deviation values first reduce sharply with an increase in the impeller rotational speed till the system attain the just off-bottom condition and then reduce gradually. Bohnet and Niesmak (1980) have defined a criterion to distinguish the quality of suspension in three broad regions based on these values of the standard deviation. For homogeneous suspension (defined with almost uniform concentration of solids in the vessel) the value of standard deviation is found to be smaller than 0.2 ($\sigma < 0.2$). However, for just suspension condition, the value of standard deviation lies between 0.2 and 0.8 ($0.2 < \sigma < 0.8$) and for incomplete suspension $\sigma > 0.8$. A close look at Fig. 3 shows that the standard deviation value approaches to 0.8 at an impeller rotational speed between 13.4 and 15 rps; indicating just off-bottom suspension condition was achieved. This is in good agreement with the critical impeller speed required for just off-bottom suspension (13.4 rps)estimated using the correlation proposed by Zwietering (1958) for the condition chosen in the work. However, the impeller rotational speed equal or more than 40 rps is required to achieve the homogeneous suspension in the vessel ($\sigma \leqslant 0.2$). It is, however, difficult to exactly identify the impeller speed required at which the complete suspension is achieved, from the predicted values of the standard deviation of solids concentration.

At higher concentration of solids ($\geqslant 10\%$ by volume), with increase in the impeller rotational speed, an interface appears between the suspended solids and a clear liquid layer in the upper part of

**Table 1**
Power number variation with respect to impeller speed in terms of form and skin drag

| Impeller rotational speed, $N$ (rps) | Impeller, $Re$ | Power number | | |
|---|---|---|---|---|
| | | Form drag | Skin drag | Total |
| 2 | $2 \times 10^4$ | 3.40 | 0.19 | 3.59 |
| 5 | $5 \times 10^4$ | 3.40 | 0.32 | 3.72 |
| 10 | $10 \times 10^4$ | 3.42 | 0.33 | 3.75 |
| 13 | $13 \times 10^4$ | 3.69 | 0.30 | 3.99 |
| 15 | $15 \times 10^4$ | 3.5 | 0.27 | 3.77 |
| 17 | $17 \times 10^4$ | 3.52 | 0.25 | 3.77 |
| 18.3 | $18.3 \times 10^4$ | 3.54 | 0.24 | 3.78 |
| 20 | $20 \times 10^4$ | 3.55 | 0.23 | 3.78 |
| 25 | $25 \times 10^4$ | 3.59 | 0.2 | 3.79 |
| 30 | $30 \times 10^4$ | 3.63 | 0.17 | 3.8 |
| 40 | $40 \times 10^4$ | 3.68 | 0.14 | 3.82 |

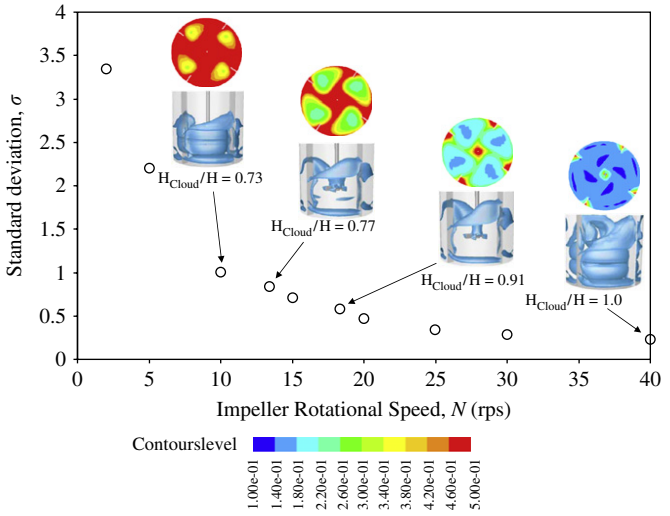


**Fig. 4.** Predicted influence of impeller rotational speed on suspension quality.

the vessel (Mak, 1992; Hicks et al., 1997; Bujalski et al., 1999). The height of this interface is the cloud height. Under this suspension condition, mixing between the suspended solids and the upper clear liquid layer is very limited and leads to high values of mixing time in the clear liquid layer as compared to the suspended solids. The cloud height is also a measure of suspension quality prevailing in the reactor. According to Kraume (1992), a state of complete suspension is achieved when the cloud height is equal to 90% ($H_{\text{cloud}} = 0.91H$) of the liquid height. Therefore the identification of the cloud height with the impeller rotational speed is very important. In the present study, the predicted iso-surfaces of the average solids concentration were monitored to analyze the variation of the cloud height with respect to the impeller rotational speed. The cloud height was defined as the distance of the highest point of the iso-surface of the average solids concentration from the bottom of the reactor. The predicted cloud heights for four impeller rotational speeds ($N = 10$, 13.4, 18.3 and 40 rps) are shown in Fig. 4. The computational model has captured the increase in the cloud height with an increase in the impeller rotational speed. It can be seen from Fig. 4 that, based on the criteria proposed by Kraume (1992), the impeller rotational speed required to achieve the complete suspension condition lies around 18.3 rps ($H_{\text{cloud}} = 0.91H$ for 18.3 rps), which is in good agreement with the experimental observations ($N = 18.3$ rps) of Yamazaki et al. (1986).

Thus, the computational model used in the present work was able to capture the solid hold-up distribution and the influence of

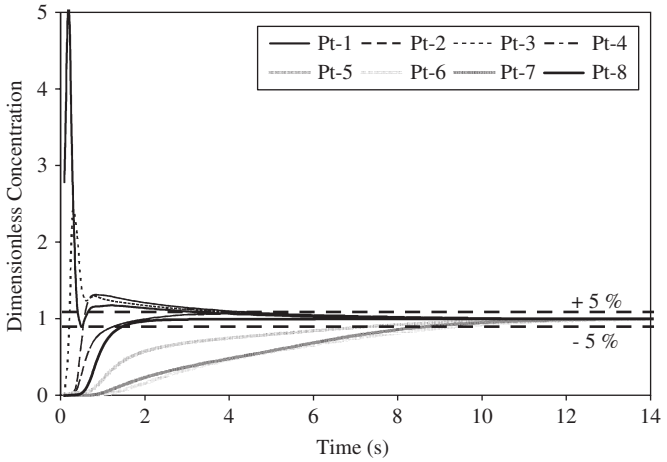


**Fig. 5.** Mixing time calculations based on the predicted tracer concentration profile for $N = 15$ rps.

impeller rotational speed on the suspension quality prevailing in the reactor both qualitatively and quantitatively. The computational model was then extended to understand the implications of the prevailing suspension quality on the liquid-phase mixing process.

### 3.2. Liquid-phase mixing

Completely converged solid–liquid flow results were then used for simulating the liquid-phase mixing, assuming that the addition of tracer does not influence the fluid dynamics in the stirred reactor. In order to simulate liquid-phase mixing process the mass fraction of the tracer equal to one was patched over 1% of reactor volume at the beginning to mimic instantaneous addition of the tracer. The species transport equations were solved till the desired mixing was achieved. The time step used for all the simulation was 0.001 s with 20 internal iterations. The "mixing time" is defined, as the time required for achieving the specified degree of homogeneity from the time at which the tracer is added to the reactor. Ranade et al. (1991) have discussed various definitions to calculate mixing time. In the present study, the mixing time is calculated from the tracer concentration history recorded at eight different locations in the reactor as shown in Fig. 5. Out of the eight locations, four locations were selected near the top surface (Pt-5, Pt-6, Pt-7 and Pt-8) so as to capture the effects of delayed mixing in the top clear liquid layer. The mixing time for each selected location was calculated as the time required for the tracer concentration to lie within (±5%) of the final concentration ($C_\infty$). The maximum value of the mixing time obtained from all the eight different locations was considered as the effective mixing time of the system.

In the previous section we have seen that different suspension quality prevails in the reactor depending on the impeller rotational speed. The liquid-phase mixing process was simulated for 11 impeller rotational speed starting from $N$=2 to 40 rps. As discussed earlier, for the present setup, the homogeneous suspension is achieved at an impeller speed $N = 40$ rps and hence the mixing process was simulated at such a high impeller speed only to study the effect of suspension quality on the mixing process. Fig. 6 shows the variation of dimensionless mixing time $N\theta$, with impeller rotational speed. The dimensionless mixing time was found to first increase sharply, reach a maximum value and then drops slowly. It can be seen from Fig. 6 that the system shows a minimum value of dimensionless mixing time (i.e., faster mixing) for the lowest impeller rotational speed equal to 2 rps. The predicted flow characteristics were closely examined to understand the possible reasons for the observance of faster

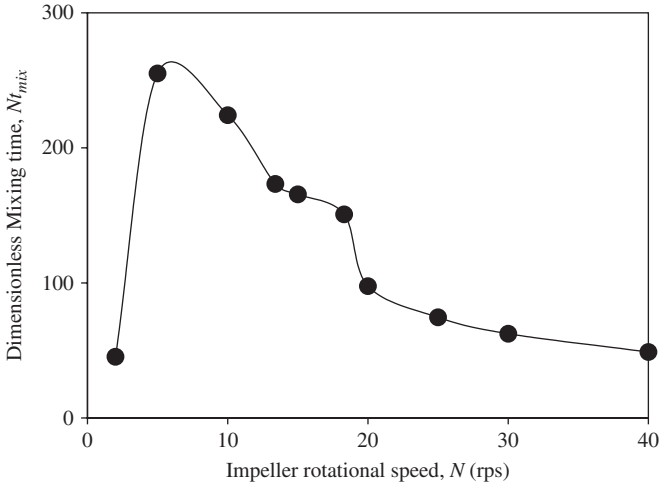


**Fig. 6.** Predicted influence of impeller rotational speed on liquid-phase mixing and power number for $\alpha = 0.1$, $d_p = 264\,\mu m$.

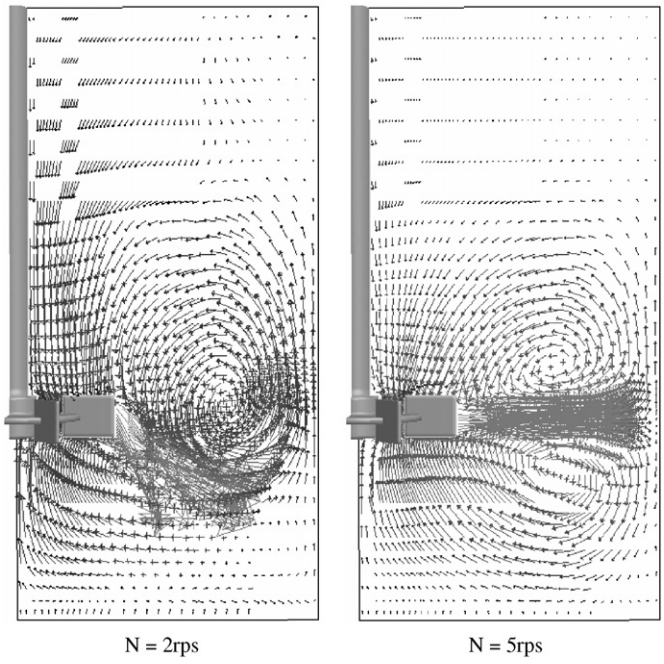


**Fig. 7.** Predicted influence of solids on the liquid-phase flow pattern.

liquid mixing for the lowest impeller speed. The predicted liquid flow pattern, shown in Fig. 7, indicates the presence of single loop flow pattern in the reactor. At such low impeller rotational speed, all the solids were found to present at the bottom of the reactor (see iso-surface of solids concentration for $N = 2$ rps shown in Fig. 4). The presence of solid bed at the bottom of the reactor offers an apparent low clearance (i.e., false bottom effect) to the impeller-generated flow and therefore leads to a single-loop fluid flow pattern even with a radial flow impeller. Galleti et al. (2003) have also observed the transition of two-loop structure to single-loop structure for a radial flow impeller with a decrease in the impeller off-bottom clearance. In a solid–liquid stirred reactor, when the solids are suspended, the energy dissipated by an impeller is used for generating liquid circulatory circulations (i.e., liquid mixing), at the solid–liquid interface for keeping solids in suspension. At the lowest impeller speed, $N = 2$ rps, no solids are suspended off the vessel bottom which means no additional drag on the moving liquid and all the energy dissipated by an impeller was available for generating liquid circulations which consequently leads to faster mixing.

With an increase in the impeller rotational speed the dimensionless mixing time increases, reaches a maximum and then again decreases (see Fig. 6). The maxima in the mixing time occurs at around $N = 5$ rps. This maxima is related to change in the liquid-phase flow pattern and the suspension quality prevailing at $N = 5$ rps. With an increase in the impeller rotational speed (up to $N = 5$ rps), solids start suspending off the vessel bottom (see Fig. 4) and the so-called *false bottom effect* vanishes, resulting into the well-known two-loop flow pattern, characteristics of the radial flow impeller (see Fig. 7). For two-loop flow pattern the rate of exchange between the two loops limits the fluid mixing process. Also as the solids are suspended in the liquid volume, some part of the fluid energy is dissipated at the solid–liquid interface and hence due to less energy availability for the fluid mixing process thereby increases the fluid mixing time of the system.

As said earlier, the previously reported literature highlighted the discrepancy over the operating conditions at which the said maxima in the mixing time occur. In the present study, the maxima in the mixing time has been observed at $N = 5\,\text{rps} = \frac{1}{3}N_{CS}$. (It should be noted that the predicted $N_{CS}$ for this system is 18.3 rps.) This operating range for highest mixing time obtained using the developed computational model is in good agreement with the experimental study of Michelletti et al. (2003). Further increase in the impeller rotational speed leads to a reduction in the mixing time (increase in the mixing efficiency). This observed reduction in the mixing time persists till the system achieved the complete suspension condition i.e., till $N = N_{CS} = 18.3$ rps. The operating conditions (impeller speed) beyond the $N_{CS}$ shows almost same mixing efficiency (constant value of dimensionless mixing time) till $N = 25$ rps (see Fig. 6). This may be because of the fact that, beyond $N_{CS}$ rate of the transport process increases very slowly. Beyond $N = 25$ rps the dimensionless mixing time decreases gradually with an increase in the impeller rotational speed. This could be because of the reason that, beyond $N = 25$ rps the solids are suspended up to top of the reactor and the clear liquid region has almost vanished (see Fig. 4) and the system shows a behavior, similar to the single-phase stirred reactor.

### 3.3. Mixing in top clear liquid layer

The predicted results were further used to understand the contribution of mixing in the top clear liquid layer on the overall mixing process. The variation in the mixing time values at four locations, two in fastest mixing region i.e., the impeller discharge stream (Point 1 and 3 in Fig. 1) and two in slowest mixing region i.e., near top surface (Point 5 and 6 in Fig. 1) have been used to explain the delayed mixing in clear liquid layer. Fig. 8 shows variation in mixing time at these four locations with respect to impeller speed with different suspension conditions. It can be seen from Fig. 8 that the difference between the predicted values of mixing time near impeller discharge stream and near the top surface are dependent on the overall suspension quality in the reactor. It was observed that for incomplete as well as for complete off-bottom suspension regimes, the mixing time values in clear liquid layer have been found to be significantly higher (2–2.5 times) than the mixing time values in the slurry. However, the difference between the mixing time values of all the four locations decreases after the system has reached the complete suspension regime.

Kraume (1992) and Bujalski et al. (1999) have postulated that the delayed mixing in the clear liquid layer is because of the very low liquid velocities in the top clear liquid layer. The predicted results were then further checked to understand the influence of the presence of solids on the liquid-phase velocities. The predicted liquid-phase

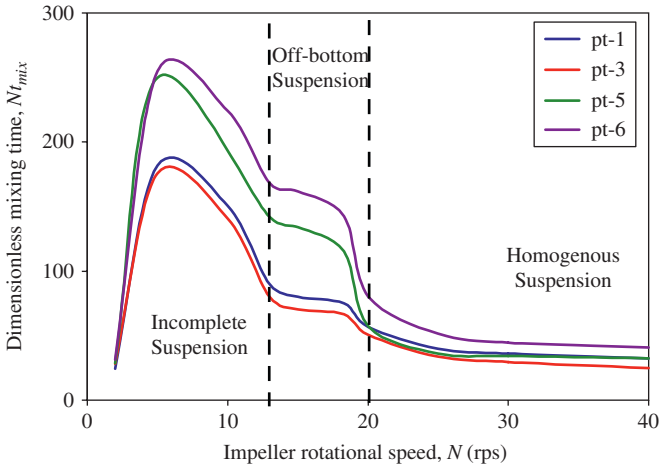


**Fig. 8.** Predicted influence of suspension quality on delayed mixing in top clear liquid layer.

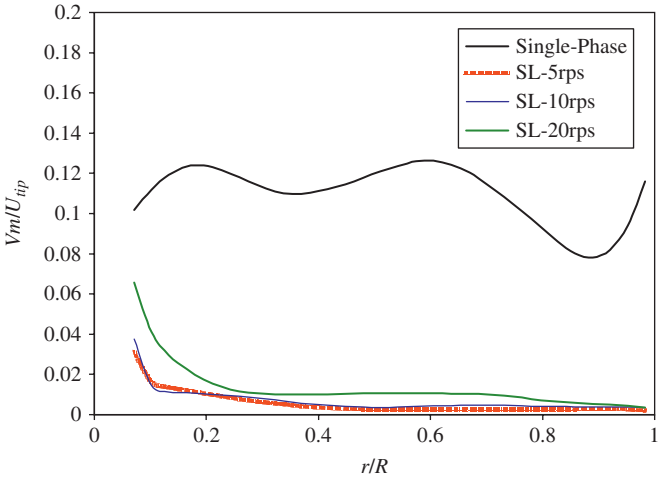


**Fig. 9.** Comparison of normalize liquid-phase velocity magnitudes near top surface, for $d_p = 264\,\mu$m.

velocity magnitudes were compared with the single-phase stirred tank results at an axial height of 0.28 m from the bottom of the reactor. The comparison of liquid-phase velocity magnitudes is shown in Fig. 9. It can be seen from Fig. 9 that the computational model has predicted significant reduction in liquid velocity values for solid–liquid flows near the top surface as observed in the experiments (Geisler and Mersmann, 1988). In a stirred reactor, of the total energy delivered to the system, approximately 50% of the energy is dissipated in the impeller discharge region. For a stirred slurry reactor, additional 25% of the energy is dissipated at the solid–liquid interface. This means that the fluid accelerated by the impeller looses about 75% of its momentum in the dense slurry before reaching to the top clear liquid layer. Therefore, less energy is available for liquid circulation in the top clear liquid layer, reducing the liquid velocities in the top clear layer. Fig. 9 also shows that the liquid velocities (in the top clear layer) are lowest for $N = 5$ rps, thus explaining the maximum mixing time at $N = 5$ rps. This indicates that the delayed mixing observed in the clear liquid layer (above the suspension) is the major source for the higher mixing times observed in the stirred slurry reactor.

Overall, it can be said that the liquid-phase mixing process occurring in the reactor is controlled by the prevailing suspension quality in the reactor. The computational model developed in the present study successfully captured the influence of suspension quality on liquid-phase mixing qualitatively.

## 4. Conclusions

A computational fluid dynamics (CFD) based model has been developed to understand the complex interaction between solid suspension quality and the liquid-phase mixing process in a stirred slurry reactor. The two-fluid model along with the standard $k$–$\varepsilon$ model of turbulence with mixture properties was used to simulate solid–liquid flows in a stirred slurry reactor. The model was further extended to understand the influence of suspension quality on the liquid-phase mixing process occurring in the stirred slurry reactor. Key conclusions based on this work are listed as follows:

1. The mixing time increases with an increase in the impeller rotational speed, reaches a maximum value then drops gradually with further increase in the impeller rotational speed till the just off-bottom suspension condition is reached. The mixing time was then found to remain constant till the system approaches a complete suspension condition and then the mixing time slowly reduces with further increase in the impeller rotational speed.
2. The computational model has predicted maxima in the mixing time at $\frac{1}{3}N_{CS}$. The maximum mixing time was found to be almost 10 times the minimum value of the mixing time obtained at $N =$ 40 rps.
3. The delayed mixing occurring in the top clear liquid is responsible for the increase in the mixing time.
4. The presence of very low liquid velocities in the top clear liquid layer is responsible for the delayed mixing.

Thus, the developed computational model has successfully captured the key features of the liquid-phase mixing process in the solid–liquid stirred reactor. The model and results presented in this work useful for extending the application of the CFD model for simulating the solid suspension and liquid-phase mixing process in large scale stirred slurry reactors. The present work, therefore, makes a useful contribution to understand complex flow processes occurring in stirred slurry reactors.

## Notation

| | |
|---|---|
| $C$ | impeller off-bottom clearance, m |
| $C_D$ | drag coefficient in turbulent liquid |
| $C_{D0}$ | drag coefficient in still liquid |
| $C_{\text{lift}}$ | lift coefficient |
| $d_p$ | particle diameter, m |
| $D_i$ | impeller diameter, m |
| $D_{12}$ | turbulent diffusivity, $m^2/s$ |
| $F_D$ | inter-phase drag force, $N/m^3$ |
| $g$ | acceleration due to gravity, $m/s^2$ |
| $G$ | turbulence generation, $kg\,m/s^3$ |
| $H$ | reactor height, m |
| $H_{\text{cloud}}$ | cloud height, m |
| $k$ | turbulent kinetic energy, $m^2/s^2$ |
| $N$ | impeller rotational speed, rps |
| $p$ | pressure, $N/m^2$ |
| $r$ | radial coordinate, m |
| $Re_p$ | particle Reynolds number |
| $S_\phi$ | source term for $\phi$ |
| $t$ | time, s |
| $T$ | reactor diameter, m |
| $U$ | velocity, m/s |

| | |
|---|---|
| $U_{tip}$ | impeller tip speed, m/s |
| $V$ | volume of reactor, $m^3$ |
| Vm | velocity magnitude, m/s |
| $x$ | position vector, m |
| $z$ | axial coordinate, m |

*Greek letters*

| | |
|---|---|
| $\alpha$ | volume fraction |
| $\varepsilon$ | turbulent kinetic energy dissipation rate, $m^2/s^3$ |
| $\lambda$ | Kolmogorov length scale, m |
| $\mu$ | viscosity, kg/m s |
| $\rho$ | density, $kg/m^3$ |
| $\sigma$ | standard deviation |
| $\tau$ | shear stress, $N/m^2$ |

*Subscripts*

| | |
|---|---|
| 1 | liquid |
| 2 | solid |
| $q$ | phase number |
| $t$ | turbulent |

## References


Angst, R., Harnack, E., Singh, M., Kraume, M., 2003. Grid and model dependency of the solid/liquid two-phase flow CFD simulation of stirred reactors. In: Proceedings of 11th European Conference of Mixing, Bambarg.

Baldyga, J., Pohorecki, R., 1995. Turbulent micromixing in chemical reactors—a review. The Journal of Chemical Engineering 58, 183–195.

Barrue, H., Bertrand, J., Cristol, B., Xuereb, C., 2001. Eulerian simulation of dense solid–liquid suspension in multi-stage stirred reactor. Journal of Chemical Engineering of Japan 34 (5), 585–594.

Bohnet, M., Niesmak, G., 1980. Distribution of solids in stirred suspensions. German Chemical Engineering 3, 57–65.

Brucato, A., Grisafi, F., Montante, G., 1998. Particle drag coefficient in turbulent fluids. Chemical Engineering Science 45, 3295–3314.

Bujalski, W., Takenaka, K., Paolini, S., Jahoda, M., Paglianti, A., Takahashi, K., Nienow, A.W., Etchells, A.W., 1999. Suspension and liquid homogenization in high solids concentration stirred chemical reactors. Chemical Engineering Research and Design 77, 241–247.

Derksen, J.J., 2003. Numerical simulation of solid suspension in a stirred tank. A.I.Ch.E. Journal 49, 2700–2714.

Galleti, C., Brunazzi, E., Yianneskis, M., Paglianti, A., 2003. Spectral and wavelet analysis of the flow pattern transition with impeller clearance variations in a stirred vessel. Chemical Engineering Science 58, 3859–3875.

Geisler, R.K., Mersmann, A.B., 1988. Local velocity distribution and power dissipation rate of suspension in stirred vessels. In: 6th European Conference on Mixing, Pavia, Italy, pp. 267–272.

Harrop, K.L., Spanfelner, W.H., Jahoda, M., Otomo, N., Etchells, A.W., Bujalski, W., Nienow, A.W., 1997. Impact of suspended solids on the homogenization of the liquid phase under turbulent conditions in stirred vessel. In: 9th European Conference on Mixing, pp. 41–48.

Hicks, M.T., Myers, K.J., Bakker, A., 1997. Cloud height in solids suspension agitation. Chemical Engineering Communications 160, 137–155.

Jenne, M., Reuss, M., 1999. A critical assessment on the use of $k$–$\varepsilon$ turbulence model for simulation of turbulent flow induced by a Rushton turbine in a baffled stirred tank reactor. Chemical Engineering Science 54, 3921–3941.

Khopkar, A.R., Kasat, G.R., Pandit, A.B., Ranade, V.V., 2006. CFD simulation of solid suspension in stirred slurry reactor. Industrial and Engineering Chemistry Research 45, 4416–4428.

Kraume, M., 1992. Mixing times in stirred suspensions. Chemical Engineering Technology 15, 313–318.

Ljungqvist, M., Rasmuson, A., 2001. Numerical simulation of the two-phase flow in an axially stirred reactor. Chemical Engineering Research and Design 79, 533–546.

Mak, A.T.C., 1992. Solid-liquid mixing in mechanically agitated vessels. Dissertation, University College, London.

Michelletti, M., Nikiforaki, L., Lee, K.C., Yianneskis, M., 2003. Particle concentration and mixing characteristics of moderate-to-dense solid–liquid suspensions. Industrial Engineering Chemistry Research 42, 6236–6249.

Montante, G., Magelli, F., 2005. Modelling of solids distribution in stirred tanks: analysis of simulation strategies and comparison with experimental data. International Journal of Computational Fluid Dynamics 19, 253–262.

Ranade, V.V., 1992. Numerical simulation of dispersed gas–liquid flows. Sadhana 17, 237–273.

Ranade, V.V., 2002. Computational Flow Modelling for Chemical Reactor Engineering. Academic Press, New York.

Ranade, V.V., Bourne, J.R., Joshi, J.B., 1991. Fluid mechanics and blending in agitated tanks. Chemical Engineering Science 46, 1883–1893.

Simonin, C., Viollet, P.L., 1998. Prediction of an oxygen droplet pulverization in a compressible subsonic conflowing hydrogen flow. Numerical Methods for Multiphase Flows 1, 65–82.

Van Dierendonck, L.L., Fortuin, J.M.H., Venderbos, D., 1968. The specific contact area in gas-liquid reactors. Chemical Reaction Engineering Symposium, pp. 205–213.

Yamazaki, H., Tojo, K., Miyanami, K., 1986. Concentration profiles of solids suspended in a stirred tank. Powder Technology 48, 205–216.

Zwietering, T.N., 1958. Suspending of solid particles in liquid by agitation. Chemical Engineering Science 8, 244–253.